

ALMOST ALL OF *Kepler*'S MULTIPLE PLANET CANDIDATES ARE PLANETS

JACK J. LISSAUER¹, GEOFFREY W. MARCY², JASON F. ROWE^{1,3}, STEPHEN T. BRYSON¹, ELISABETH ADAMS⁴, LARS A. BUCHHAVE^{5,6}, DAVID R. CIARDI⁷, WILLIAM D. COCHRAN⁸, DANIEL C. FABRYCKY^{9,10}, ERIC B. FORD¹², FRANCOIS FRESSIN⁴, JOHN GEARY⁴, RONALD L. GILLILAND¹³, MATTHEW J. HOLMAN⁴, STEVE B. HOWELL¹, JON M. JENKINS^{1,3}, KAREN KINEMUCHI^{1,14}, DAVID G. KOCH¹, ROBERT C. MOREHEAD¹², DARIN RAGOZZINE⁴, SHAWN E. SEADER^{1,3}, PETER G. TANENBAUM^{1,3}, GUILLERMO TORRES⁴, JOSEPH D. TWICKEN^{1,3}

ApJ in press

ABSTRACT

We present a statistical analysis that demonstrates that the overwhelming majority of *Kepler* candidate multiple transiting systems (multis) indeed represent true, physically-associated transiting planets. Binary stars provide the primary source of false positives among *Kepler* planet candidates, implying that false positives should be nearly randomly-distributed among *Kepler* targets. In contrast, true transiting planets would appear clustered around a smaller number of *Kepler* targets if detectable planets tend to come in systems and/or if the orbital planes of planets encircling the same star are correlated. There are more than one hundred times as many *Kepler* planet candidates in multi-candidate systems as would be predicted from a random distribution of candidates, implying that the vast majority are true planets. Most of these multis are multiple planet systems orbiting the *Kepler* target star, but there are likely cases where (a) the planetary system orbits a fainter star, and the planets are thus significantly larger than has been estimated, or (b) the planets orbit different stars within a binary/multiple star system. We use the low overall false positive rate among *Kepler* multis, together with analysis of *Kepler* spacecraft and ground-based data, to validate the closely-packed Kepler-33 planetary system, which orbits a star that has evolved somewhat off of the main sequence. Kepler-33 hosts five transiting planets with periods ranging from 5.67 to 41 days.

Subject headings: planetary systems; stars: individual (Kepler-33/KOI-707/KIC 9458613); methods: statistical

1. INTRODUCTION

Roughly one-third of *Kepler*'s planet candidates announced by Borucki et al. (2011) are associated with targets that have more than one candidate planet. False positives (FPs) plague ground-based transit searches, but the exquisite quality of *Kepler* photometry, combined with the ability to measure small deviations in center of light during transits (Jenkins et al. 2010; Batalha et al. 2010), have been used to cleanse the sample prior to presentation in Borucki et al. (2011). Accounting for candidates on each one's individual merit, Morton & Johnson

(2011) estimated the fidelity of *Kepler*'s planet candidates (fraction of the candidates expected to be actual planets) to be above 90%. Yet the fidelity of multiple planet candidates is likely to be higher than that for singles (Latham et al. 2011; Lissauer et al. 2011a). We show herein that the vast majority of *Kepler*'s multiple planet candidates are true multiple planet systems.

The majority of *Kepler* planet discoveries announced to date have been confirmed dynamically, using radial velocity variations of the target star or departures of observed transit times from a linear ephemeris (transit timing variations, TTVs). However, three of the first sixteen *Kepler* planets do not have dynamical evidence supporting the discovery, but rather these planets have been "validated" by showing that the probability that the observed signal is produced by a planet around the host star is at least 100 times as large as that of a false positive (Torres et al. 2011; Fressin et al. 2011; Lissauer et al. 2011b). For these three planets, the validation process was based on the results of the BLENDER code, which performs detailed comparisons between the observed *Kepler* lightcurve and the lightcurves predicted for an ensemble of theoretically conceivable FPs to reject FP models that are not consistent with the observations. BLENDER then sums the *a priori* probability for the allowed false positives and compares that to the *a priori* probability for the planet model. BLENDER validates a planet when the resulting odds ratio very strongly favors the planet model. Although all three of these planets orbit stars that also have dynamically-confirmed planets, planetary multiplicity was not used quantitatively to aid in their validation.

Jack.Lissauer@nasa.gov

¹ NASA Ames Research Center, Moffett Field, CA 94035, USA

² Astronomy Department, University of California, Berkeley, CA 94720, USA

³ SETI Institute/NASA Ames Research Center, Moffett Field, CA 94035, USA

⁴ Harvard-Smithsonian Center for Astrophysics, 60 Garden Street, Cambridge, MA 02138, USA

⁵ Niels Bohr Institute, University of Copenhagen, DK-2100, Copenhagen, Denmark

⁶ Centre for Star and Planet Formation, Natural History Museum of Denmark, University of Copenhagen, DK-1350 Copenhagen, Denmark

⁷ Exoplanet Science Institute/Caltech, Pasadena, CA 91125, USA

⁸ Department of Astronomy, University of Texas, Austin, TX 78712, USA

⁹ Department of Astronomy & Astrophysics, University of California, Santa Cruz, CA 95064, USA

¹⁰ Hubble Fellow

¹¹ University of Florida, 211 Bryant Space Science Center, Gainesville, FL 32611, USA

¹² Space Telescope Science Institute, Baltimore, MD 21218, USA

¹³ Bay Area Environmental Institute, CA

Morton & Johnson (2011) do a more cursory analysis, but one that is far easier, enabling them to perform it for all of the candidate planets (“candidates”, henceforth) that are listed in the Borucki et al. (2011) paper. The study by Morton & Johnson (2011) assumes a flat 20% planet occurrence rate as a prior for their Bayesian analysis (i.e., the average number of planets per star is assumed to be 0.2), and they do not consider planets orbiting background stars to be FPs. Morton & Johnson (2011) use the depth and period of the transit, together with the magnitude, stellar properties and galactic latitude of the target star (henceforth “target”) to provide an upper bound on the FP prior; for high SNR transits, this upper bound on the FP prior can be much higher than the one computed using detailed lightcurve matching by BLENDER to rule out many FP scenarios (Torres et al. 2011; Fressin et al. 2011). Indeed, Morton & Johnson (2011) do not examine *Kepler* lightcurves, but rather assume for their calculations that various false-positive vetting procedures using *Kepler* photometry have been done, such as elimination of candidates with V-shaped lightcurves or where the centroid of light received on the *Kepler* focal plane is in a different position during a transit than it is outside of transit, and that the planet candidates show no evidence for being FPs. However, these cuts were not applied to all of the candidates listed in Borucki et al. (2011). Some candidates were not vetted as extensively as assumed by Morton & Johnson (2011), and other candidates did not pass one of the cleanness tests but still remain viable, if somewhat more suspect, planetary candidates (e.g., grazing planetary transits, as well as grazing stellar eclipses, produce V-shaped lightcurves), and thus remain on Borucki et al. (2011)’s candidate list.

We develop herein a quantitative method to estimate the true planet fraction of the overall sample of *Kepler* candidate multiple planets that is based upon the observation that there are far more multiples than would be expected for a random distribution of candidates among *Kepler* targets (Lissauer et al. 2011a). This “overabundance” of multiples is illustrated by the fact that fewer than 1% of targets have a candidate on Borucki et al. (2011)’s candidate list, whereas more than 15% of targets with at least one candidate have multiple candidates, and more than 25% of targets with at least two candidates have a third candidate. Such a result is expected if planets often appear within systems of planets, especially if such systems tend to be flat in the distribution of inclinations. High multiplicity, low inclination, planetary systems are consistent with *Kepler* observations (Lissauer et al. 2011a).

We describe an approach to validation of specific multiple planet system candidates that is intermediate between those of Morton & Johnson (2011) and BLENDER, and we apply these techniques to validate the very flat and dynamically-packed KOI-707 system¹⁴. In this approach, applied herein exclusively to KOI-707, we exam-

ine the target and candidates individually, supplementing the *Kepler* Input Catalog (KIC, Brown et al. 2011) with spectroscopic observations of the target and high-resolution imaging, including Keck guider camera exposures and speckle imaging (Howell et al. 2011) and/or adaptive optics (Troy et al. 2000; Hayward et al. 2001), to search for other stars in the target aperture. We check the lightcurve for a shape consistent with a transit. We verify that the centroid motion is nil or consistent with a transit around the target star and not a transit/ eclipse of any other stars observed nearby. But we do not perform detailed matching of observed lightcurves to FP scenarios. We then use multiplicity to effectively increase the planet priors and allow for validation in a Bayesian sense. Note that for candidate giant (~ 1 Jupiter radius) planets, one would need to consider the possibility of the transit signal being produced by a late M star partially eclipsing the target star (perhaps with dilution); for smaller candidates, the possibility of transits of fainter stars by larger planets must be taken into account.

The probability of a candidate in a multiple system being a false positive is contrasted to that of a single candidate in Section 2. Other factors involved in validating transiting planet candidates are discussed in Section 3. We apply our method to the KOI-707 candidate multiple planet system in Section 4. We conclude in Section 5 with a summary of our results and a discussion of their implications.

2. STATISTICAL VALIDATION OF MULTI-PLANET CANDIDATES

Kepler has found far more multiple candidate systems than would be the case if candidates were randomly distributed among target stars (Lissauer et al. 2011a). False positives are expected to be nearly randomly distributed among *Kepler* targets, whereas true transiting planets could be clustered if planets whose sizes and periods are adequate for transits to be detected often come in multiples, as is the case for planets detected by radial velocity variations (Wright et al. 2009), and/or if planetary systems tend to be flat, so geometry leads to higher transit probabilities for other planets if one planet is seen to transit (Ragozzine & Holman 2010). We quantify the excess of multiples and its implications for the overall fidelity of the sample of multiple candidates in this section.

We use the following notation and input parameters: The number of planet candidates is $n_c = 1199$, the number of targets with two or more candidates, i.e., the number of candidate multiple planet systems, is $n_m = 170$, and the number of targets from which the sample is drawn is $n_t = 160,171$. These numerical values are taken from Lissauer et al. (2011a), who removed from the 1235 candidates listed in Borucki et al. (2011) those objects that were estimated to have radii greater than twice that of Jupiter, those for which only one transit had been observed, and those identified as FPs by Howard et al. (2011). We denote the number of actual planets among the candidates as n_p , the number of false positives as n_f , and the fidelity of the sample (fraction of candidates that are planets) as P , so $n_c = n_p + n_f$ and $P = n_p/n_c$.

For our calculations in Equations (1–9), we make the following two assumptions:

i) FPs are randomly distributed among the targets;

¹⁴ Targets with planetary candidates are given an integer KOI (*Kepler* Object of Interest) number, and individual candidates are denoted by the target KOI number followed by a decimal point and a two digit number specifying the order in which they were identified. For example, KOI-707.02 is the second planetary candidate to have been identified by transit-like signatures in the lightcurve of the target star KOI-707.

ii) there is no correlation between the probability of a target to host one or more detectable planets and to display FPs.

In contrast, we do not assume that planets are randomly distributed among the targets. The previous verifications of the two-planet *Kepler*-10 system (Batalha et al. 2011; Fressin et al. 2011), the three-planet *Kepler*-9 (Holman et al. 2010; Torres et al. 2011) and *Kepler*-18 systems (Cochran et al. 2011), and especially the six-planet *Kepler*-11 system (Lissauer et al. 2011b), provide strong evidence of the non-random distribution of transiting planets among *Kepler* target stars.

The above two assumptions, together with observed values of n_c , n_m and n_t and an assumed lower bound on P , allow us to estimate lower bounds on the fidelity of candidates in various classes of candidate multi-planet systems using simple algebra. For example, assumption (1) implies that the expected number of targets with k false positives, $E(k)$, is given by a Poisson distribution of n_t members whose mean is given by the average number of false positives per target, $\lambda = (1 - P)n_c/n_t$. This expectation value is given by the following formula:

$$E(k) = \frac{\lambda^k e^{-\lambda}}{k!} n_t = \frac{((1 - P)\frac{n_c}{n_t})^k e^{-(1-P)\frac{n_c}{n_t}}}{k!} n_t \quad (1)$$

$$\approx \frac{((1 - P)\frac{n_c}{n_t})^k}{k!} n_t,$$

where the approximation in Equation (1) is valid for $\lambda \ll 1$.

We next compute the expected number of *Kepler* targets with multiple candidates at least one of which is a FP. In some cases, we make approximations that yield conservative estimates of the expected numbers of true planets (i.e., overestimate the expected number of FPs). Our results, presented in Equations (2–7), are given first as general formulae, then as a function of the fraction of candidates that are true planets, P , for the observed values of 160,171 targets, 1199 candidates, and 170 multiple candidate systems stated above, and finally these value if $P = 0.5$ or 0.9^{15} . These final numbers are to be compared to the observation that there are 115 candidate 2-planet systems, with a total of 230 planet candidates, and 55 candidate systems of 3 or more transiting planets, with a total of 178 planet candidates.

Equation (1) yields estimates of the number of targets with two or three false positives:

$$2 \text{ FPs} : \frac{((1 - P)n_c)^2}{2n_t} = 4.49(1 - P)^2 \quad (2)$$

$$= 1.12 \text{ or } 0.045;$$

$$3 \text{ FPs} : \frac{((1 - P)n_c)^3}{6n_t^2} = 0.011(1 - P)^3 \quad (3)$$

$$= 0.0014 \text{ or } 1.1 \times 10^{-5}.$$

¹⁵ We choose to present numerical results for $P = 0.9$ because we consider it to be a reasonable estimate of the actual planet fidelity rate, and $P = 0.5$ to show that even for an overall FP rate far higher than studies suggest, the expected number of FPs among the multis is remarkably low.

The number of targets expected to have four or more false positives is very small and can be neglected for our purposes. Equation (1) also yields the expected number of targets with a single FP under the same assumptions, 597.3 or 119.8.

The assumed lack of correlation between the propensity of a target to have false positives and true planets implies that the probability that a given target hosts both a planet and one or more false positive is equal to the product of these individual probabilities. The probability of a target having a detected transiting planet is given by Pn_c/n_t , and the probability of it showing a false positive is given by Equation (1). Thus, the estimated numbers of targets with at least one planet as well as one or more false positives are given by:

$$1 \text{ planet} + 1 \text{ FP} : \frac{n_c P}{n_t} \times \frac{n_c(1 - P)}{n_t} \times n_t \quad (4)$$

$$= P(1 - P) \frac{n_c^2}{n_t}$$

$$= 8.98P(1 - P) = 2.25 \text{ or } 0.81;$$

$$1 \text{ planet} + 2 \text{ FPs} : P(1 - P)^2 \frac{n_c^3}{2n_t^2} \quad (5)$$

$$= 0.034P(1 - P)^2$$

$$= 0.0042 \text{ or } 3 \times 10^{-4}.$$

The number of targets expected to have both a planet and three or more false positives is very small and can be neglected for our purposes. Somewhat lower estimates of the number of multi-candidate systems with one planet and at least one FP than given by Equations (4) and (5) can be derived by noting that the observed multiplicity implies fewer (than n_c) targets with a nonzero number of planet candidates.

To derive an estimate of the expected number of targets with multiple true planets as well as at least one FP, replace the term in Equations (4) and (5) that represents the probability of a given target having a true planet, Pn_c/n_t , with a term representing the probability of a given target having a multi-planet system, n_m/n_t . (Assuming all multis are multi-planet systems to estimate of this term is conservative in the sense that it may lead to an overestimate in the number of false positives in multi-candidate systems.)

$$2 \text{ or more planets} + 1 \text{ FP} : \frac{n_m}{n_t} \times \frac{n_c(1 - P)}{n_t} \times n_t \quad (6)$$

$$= (1 - P) \frac{n_m n_c}{n_t} = 1.27(1 - P)$$

$$= 0.64 \text{ or } 0.13;$$

$$2 \text{ or more planets} + 2 \text{ FPs} : \frac{n_m}{n_t} \times (1 - P)^2 \times \frac{n_c^2}{2n_t} \quad (7)$$

$$= 0.0048(1 - P)^2$$

$$= 0.0012 \text{ or } 5 \times 10^{-5}.$$

The number of targets expected to have both multiple

planets and three or more false positives is extremely small and can be neglected for our purposes.

2.1. Numerical Estimates for *Kepler* Candidates

Adding up the above estimates of FPs of different types yields expected totals of 4.5 or 0.9 FPs (for assumed FP rates of 50% and 10%, respectively) in doubles (compared to a total of 230 candidates) and 0.65 or 0.13 FPs in systems with three or more candidates (compared to a total of 178 candidates). These numbers suggest that validation of doubles at the 99% level by this method alone is marginal. Triples and higher multiplicity candidates are more strongly validatable, enough so that the one dynamically-unstable candidate triple system noted by Lissauer et al. (2011a), KOI-284, which has a pair of candidates with a period ratio 1.0383, should be viewed as somewhat surprising (but see Section 2.4).

It is of interest to compare the (low) false positive rates for multis estimated in the previous paragraph with the presumed FP rates for singles upon which their calculations are based. For 50% FPs in singles, our estimates above correspond to 2% FPs in doubles (compare the first numbers at the end of equations 2 and 4 with the 230 candidates in *Kepler* candidate 2-planet systems) and 0.4% FPs for targets with three or more candidates (compare the first numbers at the end equations 3 and 5–7 with the 178 candidates in *Kepler* candidate 3 or more planet systems); for 10% FPs in singles, we estimate 0.4% FPs in doubles (compare the final numbers at the end of equations 2 and 4 with the 230 candidates in *Kepler* candidate 2-planet systems) and 0.1% for targets with three or more candidates (compare the final numbers at the end equations 3 and 5–7 with the 178 candidates in *Kepler* candidate 3 or more planet systems). These values are consistent with a “multiplicity boost” in the Bayesian prior for planets of ~ 25 for a system with one additional candidate and of ~ 100 for a system with more than one additional candidate. The probability that a target hosts a planet candidate, $1/150$, can be compared to the probability of a target that hosts one candidate hosts another, $1/6$, and that an additional candidate has been found for higher multiplicity systems, $1/3$. These latter values, together with the assumption that FPs and true planets are uncorrelated, lead to an estimate of the multiplicity boost for candidate doubles of 30, slightly larger than the value of 25 computed above, and to a somewhat reduced estimate of ~ 50 for candidates in systems of higher multiplicity.

The multiplicity boost introduced in the previous paragraph can be used to quantify the increased probability that a set of transit-like signatures represent a real transiting planet if one or more additional set of transit-like signatures are detected for the same *Kepler* target; i.e., to compute an estimate the probability of a particular candidate in a multiple candidate system being a true planet from an estimate of that candidate being a planet that does not account for multiplicity. We denote the probability of planethood of the candidate in question computed without factoring in multiplicity by P_1 and the probability of it being a planet accounting for multiplicity by P_2 if it is in a two candidate system and by P_{3+} if it is a member of a three or more candidate system. In our formulation, multiplicity effectively increases the Bayesian estimate of the planet prior but leaves the FP

prior unchanged. Thus the probability of the planet interpretation accounting for multiplicity is related to that neglecting multiplicity according to the following approximate formulae:

$$P_2 \approx \frac{25P_1}{25P_1 + (1 - P_1)} \quad (8)$$

$$\left(\approx 1 - \frac{1 - P_1}{25} \text{ for } 1 - P_1 \ll 1, \text{ and } \approx 25P_1 \text{ for } P_1 \ll 1 \right)$$

$$P_{3+} \approx \frac{50P_1}{50P_1 + (1 - P_1)} \quad (9)$$

$$\left(\approx 1 - \frac{1 - P_1}{50} \text{ for } 1 - P_1 \ll 1, \text{ and } \approx 50P_1 \text{ for } P_1 \ll 1 \right),$$

where in each case we use the smaller value computed in the previous paragraph. Rough estimates for the planet probabilities of individual *Kepler* candidate multis can be obtained by applying Expressions (8) and (9) to the estimates of planet probability by Morton & Johnson (2011); the Morton & Johnson (2011) planet probabilities are given by P_1 in the above formulae since their numbers do not account for multiplicity. Note that this multiplicity boost incorporates self-consistently both the coplanarity boost discussed in Cochran et al. (2011) and the systems boost (that planets tend to come in systems) without need to disentangle these effects.

The above calculations of the multiplicity boost do not assume that any of the candidates of the target under consideration have been confirmed or validated as planets. Does validating one or more candidate as a true planet(s) substantially increase the probability that other candidates of the same target are also planets? For realistic estimates of FP rates (e.g., 10%), the equations above show that most FPs in multis are likely to be combinations of 1 FP with one or more true planets, so validating one candidate does not substantially increase confidence in the others from a statistical viewpoint. Nonetheless, validating one candidate does eliminate some of the non-statistical issues raised in the following three subsections. In particular, if that validated candidate is shown to not only be a planet but also to orbit the *Kepler* target star, then the probability that the other candidates are physically-associated with the target increases.

2.2. Caveats

To examine the validity of the three assumptions stated above, we divide FPs into two classes, (I) chance-alignment blends such as background eclipsing binaries (BGEBS) and (II) physical triple stars (PTs), where grazing eclipses of the target star by a stellar companion are considered together with PTs for this purpose. We note that it is a matter of choice how to count cases where the transit signal is produced by a planet transiting a star other than the *Kepler* target. Larger planets transiting stars that are not physically associated with the star providing most of the target’s flux can be considered to fall within the chance-alignment blends/BGEB class of FPs (as they must be for *Kepler*’s statistical census of planets, because background stars are not in the denominator of the ratio taken to calculate the fraction of stars with

planets, so their planets must not be included in the numerator), or alternatively not be regarded as FPs when assessing individual candidates and the reliability of the sample. Planets transiting physical companions to the star providing most of the flux can either be viewed as members of the PT class of FPs or not classified as FPs; how these planets are categorized for *Kepler*'s statistical census of planets is also a matter of choice.

Assumptions (i) and (ii) lead to the following caveats:

(i): The expected number of BGEs (chance-alignment blends) that can cause FPs varies with the magnitude and galactic latitude of the target star, whereas those of PTs do not (except to the extent that the distribution of stellar types among *Kepler* targets depends somewhat on magnitude). The variations in expected BGEs act to increase the expected total number of systems with 2 or more FPs compared to the value given by the above formulae. When looking at individual candidate systems, the FP probability of those around faint targets and at low galactic latitude is larger, whereas the planetary interpretation becomes more likely for brighter targets and those at higher galactic latitude. However, the distributions in galactic latitude of the planet candidates and of the multiple candidate systems both track that of all *Kepler* targets, whereas the distribution of expected BGE FPs is quite different (Figure 1); this suggests that the fraction of candidates (both singles and multis) that are produced by BGEs is small.

The statistical analysis that we presented above does not discriminate between multiple candidates resulting from multiple planets orbiting a background star and a single candidate resulting from a single planet orbiting a background star. However, the correlations and lack thereof between the curves shown in Figure 1 also imply that the fraction of KOIs caused by single or multiple planets transiting a background star is small. In some cases, it is especially unlikely that a multiple candidate system is produced by several planets orbiting a background star, either because its largest member would be greater than planetary in size, or because the requirement of dynamical stability would imply implausibly small densities for the larger planets orbiting the fainter star. Additionally, as the fraction of giant planets among the multis is smaller than it is for the singles (Latham et al. 2011), the probability of a multi being a system of larger planets orbiting a fainter star is less than that of a single candidate orbiting a star fainter than the target.

A second class of multiple FPs can be produced from a single physical system, either a triple star with two sets of eclipses or a background star with multiple transiting planets. Triple star systems are unstable for small period ratios and produce large eclipse timing variations for moderate period ratios, so if large timing variations are not detected, we do not need to consider triple star system FPs (nor grazing eclipsing binary stars with a transiting planet) unless period ratios are large.

Quadruple star systems consisting of two pairs of eclipsing binaries (e.g., Graczyk et al. 2011) could produce a small excess probability of a pair of FPs. Such systems, as well as line of sight pairs of physically-unrelated EBs, also might be more likely to mimic planetary-depth transits because of mutual dilution of the fraction of light in the *Kepler* aperture.

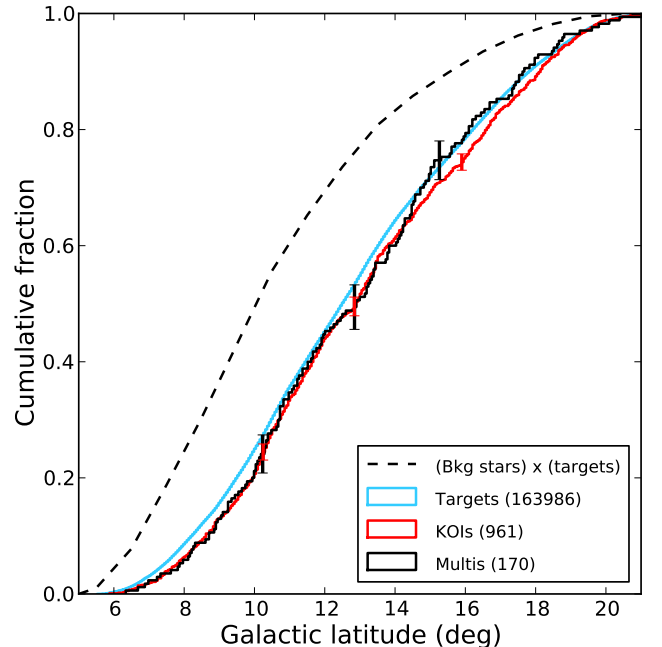


FIG. 1.— Distributions in galactic latitude of all 163,986 *Kepler* Quarter 2 exoplanet targets (solid turquoise curve), the 961 targets with planet candidates meeting our criteria (solid dark red curve) and the 170 multiple candidate systems (solid black curve). The dashed curve shows the distribution of expected BGE FPs, which we compute by weighting each target by the sky density of stars with magnitudes between 15.0 and 20.0 according to the Besancon model of the galaxy (Robin et al. 2003, 2004). All curves are normalized to give a total of unity. Error bars represent the statistical uncertainty (1σ binomial variation) of each of the planet candidate curves at quartile points in their distributions. The basic shape of the three solid curves is governed by the orientation of the *Kepler* field on the sky, where the amount of area covered increases from a point at galactic latitude 5° to a region spanning 16° in longitude at 13° in galactic latitude and then decreases to a point at 21° latitude; the second most important factor is a weighting towards the galactic plane because of the higher spatial density of target stars in that portion of the field. The dashed curve is more heavily weighted towards the galactic plane because, to first approximation, it is weighted quadratically in the spatial density of stars (more precisely, the product of the spatial densities of target stars and background stars), whereas the other curves are only weighted linearly. The spatial density of background stars drops by a factor of 17 from the lowest latitude *Kepler* observes to the highest latitude. The similarity of these curves for targets, planets and multis, and the difference of these from the curve estimating BGE FPs, suggests that the fraction of candidates that are produced by BGEs (as well as that resulting from planets transiting background stars) is small.

We note also that FPs are inherently more likely among both small (Earth-size and smaller) and large (Jupiter-size and larger) candidates than among intermediate (Neptune-size) candidates, independent of multiplicity. Most small candidates produce low-amplitude transits that reduce our ability to remove false positives from the candidate list on the basis of the shape of the lightcurve or from differences in the centroid of the location of the dip relative to that of the target. Small candidates, including multis, are more likely to be planets orbiting stars fainter than the target simply because the Neptune-

size planets that could produce such signals are far more common according to *Kepler* observations than are giant planets (Borucki et al. 2011), and this difference in abundance is even larger for the multis than for the singles (Latham et al. 2011). At the other extreme of the planet size distribution, giant candidates appear to be more contaminated by stellar false positives (Demory & Seager 2011) of the type which plague ground-based surveys than do Neptune-size candidates.

(ii): Planets and FPs of both types are more easily detectable for quieter targets; planets and PTs are more detectable for brighter targets, but BGEBs that are bright enough to mimic observable transits of the target star are more likely for fainter targets. A grazing eclipsing binary with a circumstellar or circumbinary transiting planet analogous to Kepler-16 (Doyle et al. 2011) would violate our assumption of a lack of correlation between planets and FPs, but such a configuration requires a large period ratio for stability and an even larger period ratio for the planet to have modest TTVs.

The assumption of no correlation between planets and FPs would be violated if the orientations of orbital planes of PTs with one star having a planet are not random. Alignments of planetary orbital planes for binary stars for which both stars possess planets also violate this assumption, although members of this class are true planets that are all physically associated (albeit less directly) with the target star and thus would for many purposes not be classified as FPs.

The numbers quoted in Equations (2–9) do not incorporate the caveats noted in this subsection. Correlations between the propensity of a target to have one or more FPs and to host one or more identified true planets (ii) are likely to be at most a factor of a few. False positives of the BGEB class are likely to be concentrated among faint target stars that are located at low galactic latitude (Morton & Johnson 2011); this concentration increases the expected number of targets with two (or more) FPs, but also points to a substantial portion of *Kepler*'s target list whose members have *a priori* FP likelihood that is lower than or comparable to those given by the numbers above.

2.3. Period Ratios: Resonances & Stability

The distribution of candidate period ratios exhibits spikes near strong mean motion resonances, which implies that candidates with such period ratios are more likely to be true planets than those candidates not in or very near such resonances (Lissauer et al. 2011a). This clustering can be used to increase confidence in candidates with periods near resonances; such a “near-resonance boost” can be quantified using the measured values of the normalized distance from resonance computed from the distribution of planet period ratios in Lissauer et al. (2011a). Candidate resonant planets can, however, arise from period aliases in analysis of light curves; such aliases are not of the form of the astrophysical FPs considered in this paper, and we note that special care to search for them is an important aspect of validating candidate resonant planets (see the discussion of KOI-730 and the Note Added in Proof in Lissauer et al. (2011a)).

Resonant period ratios increase confidence in various candidates, and as mentioned at the beginning of Sec-

tion 2.1, one of the candidate systems, KOI-284, is highly suspect because two of the candidates have periods that differ from one another by $< 4\%$, which would rapidly lead to a dynamical instability on a very short time scale (but see the discussion of this system in Section 2.4). Do non-resonant periods reduce the confidence in individual multis and do stable systems produce an increase in our confidence? The answers to both parts of this question are yes, but in most cases these effects are minor. While resonances are overpopulated, a substantial majority of multis are not in nor near such resonances (Lissauer et al. 2011a; Wright et al. 2011). And while drawing planetary periods randomly from the observed ensemble of transiting planet periods gives many more nominally unstable systems than are observed, the fraction of unstable configurations from such a random draw is still small. Nonetheless, in high-multiplicity densely-packed systems, wherein most configurations with the same number of planets randomly spread over the same range in period would likely be unstable, the boost in confidence from stability can be significant. Note that special period ratio boosts and stability boosts are in addition to the standard multiplicity boost, i.e., they can be applied together as two multiplicative factors in the planet prior for appropriate systems.

2.4. KOI-284 & Multis Composed of Planets Transiting Differing Stars in a Binary

A very rough estimate of the expected number of multiple candidate systems that orbit different members of a binary/multiple star system (rather than a single system of planets orbiting the same star) can be made by assuming that half of *Kepler*'s targets are binaries, that each star within a binary is as likely to host both single and multiple transiting planets as are single stars, and that the probability of one star within a binary hosting transiting planets is uncorrelated with that of its binary companion. These assumptions imply n_c planets spread around $3n_t/2$ stars, and thus $(2/3)(n_c/n_t)$ planets per star and $2n_c^2/(9n_t) \approx 2$ cases in which multis are composed of planets transiting differing members of a stellar binary. Positive correlations between the propensity of stars in a binary to have transiting planets (resulting from the abundance of planets and/or alignment of orbital planes) would increase this number, but the fact that a significant majority of binaries are composed of stars of substantially differing surface brightness combined with the paucity of giant planets transiting low luminosity stars should reduce the number of multis comprised of two planetary systems because of the difficulty of detecting planets around secondary stars.

As mentioned above, KOI-284, with three planetary candidates having periods of 6.18, 6.42, 18.0 days and nominal sizes of $\sim 2 R_\oplus$ (Earth radii), is the only one of 170 multi-candidate system identified in Borucki et al. (2011) that would be clearly dynamically unstable if all of the planets orbited the same star (Lissauer et al. 2011a)¹⁶. Analysis of a McDonald observatory spectrum of this bright (*Kepler* magnitude $Kp = 11.8$) target

¹⁶ The other multi that was unstable according to the integrations reported in Lissauer et al. (2011a) was the 4 candidate system KOI-191. This instability resulted from the strong perturbations of giant planet candidate KOI-191.01 on the nearby outermost candidate KOI-191.04. As the period ratio of these two candidates

yields a temperature of ~ 6250 K and $\log g = 4.5$, which suggest a F7V star that is twice as luminous as the Sun. Speckle images of KOI-284 obtained on 24 June 2010 revealed two stars differing in brightness by less than one magnitude and separated from one another by slightly less than $1''$ (Howell et al. 2011). Spectroscopic observations of each individual star obtained at Keck in 2011 show the two stars to have nearly identical spectra and have a difference in radial velocity of 0.94 ± 0.1 km/s. The nearly identical velocities are consistent with their being gravitationally bound. Their separation of $0.9''$ at a distance of roughly 500 pc implies a projected separation of 450 AU; the relative orbital velocities for two $1 M_{\odot}$ stars on a circular orbit with semimajor axis $a = 450$ AU is 2 km/s. These observations suggest that the three candidates may well all be transiting planets in the same stellar system, with one of the stars hosting one of the six day period planets and the other two planets orbiting the other star in the binary. Thus, this system would not call into question the statistical arguments presented in Section 2.1. A detailed analysis of both *Kepler* and ground-based data to test this hypothesis and elucidate particulars is currently underway (Bryson et al. 2012).

3. TRANSIT CHARACTERISTICS: PLANETS VS. FALSE POSITIVES

The numbers derived in Section 2 suggest that the sample of multi-planet candidates identified by Borucki et al. (2011) is likely to include only a small fraction of false positives, of order 1%. But because of the uncertainties associated with the caveats discussed in Section 2, as well as any factors that we may have omitted, we do not consider it appropriate to view all of *Kepler*'s multi-planet candidates to be validated planets at the 99% level. Nonetheless, it is possible to identify candidates with various favorable characteristics as detailed below, and to examine the available data for systems individually for signs of potential inconsistencies with the planet hypothesis. See Haswell (2011) for a more detailed discussion of transit characteristics.

The shape and duration of a candidate transit can be used to distinguish events produced by planets from false positives produced by known astrophysical sources. The BLENDER code (Torres et al. 2011) compares the observed lightcurve to synthetic lightcurves of both a planet transiting the target star and a vast array of possible astrophysical false positives involving binary stars and larger planets transiting fainter stars. If the planet hypothesis does not provide an acceptable fit to the data, the candidate is not viable; candidates for which the planet fit is marginal are called into question, and such candidates are not considered further herein. Astrophysical false positives are considered credible if they provide an acceptable fit (3σ) to the data. Then the *a priori* likelihoods of the planet hypothesis and that of a false positive are compared, and a probability that the apparent transit is caused by a blend is computed. The

was 1.258, Lissauer et al. (2011a) speculated that the system was librating in a 5:4 mean motion resonance and that this resonance protected the planets from close approaches. Subsequent data analysis shows that the period of KOI-191.04 was underestimated by a factor of two. The updated value of the period of this candidate is 38.6516 ± 0.0012 days. The revised period places the planets much farther apart, and the system is stable with the updated parameters.

process can be very involved, especially for candidates with orbital periods long enough that astrophysical false positives could plausibly be produced by objects with eccentric (not tidally-damped) orbits (Fressin et al. 2011; Lissauer et al. 2011b).

True planetary transits of the star that is the dominant source of light in the aperture are wavelength-independent (neglecting the small effects of stellar limb-darkening and contamination by flux from other stars in the aperture), whereas false positives are not (except in the unlikely case that the effective temperatures of the contributing stars are similar). By providing infrared time series spanning times of transit, the Warm Spitzer Mission can assist in the validation of many transiting planet systems. Several candidates in multiple systems have been observed, and they all exhibit achromatic transit depths, consistent with planetary signals (Desert et al. 2012).

The durations of transit-like signatures can be used to assess the probability of the planetary interpretation, especially when more than one planet candidate is present for a given target. Transit and eclipse durations depend on several factors, including the masses and radii of the two objects, the impact parameter, b , which is defined as the minimum projected separation between the center of the smaller body (planet in the case of a planetary transit) and that of the larger body (star) measured in units of the radius of the larger body, and the period and eccentricity of the orbit. Central transits (those for which the center of the transiting body passes over the center of the transited body) by a planet on a circular orbit have durations that vary as the cube root of the orbital period (Kepler 1619) and inversely to the cube root of the stellar density (Seager & Mallén-Ornelas 2003); these relationships hold for FPs as long as the bright star is substantially larger and more massive than the other body. When the system's mass is dominated by the primary but the radius of the secondary cannot be ignored, then the duration, T_{dur} , (1st contact – 4th contact, which corresponds to the values reported in Borucki et al. (2011) and in Table 3 of this paper), of a central transit for a circular orbit satisfies the following proportionality relationship:

$$T_{\text{dur}} \propto \frac{R_{\star} + R_p}{R_{\star}} P_{\text{orb}}^{1/3}. \quad (10)$$

If the transit duration is measured over the time interval when the center of the planet covers the disk of the star, the first factor on the right-hand side of Expression (10) is no longer relevant and the proportionality is simply to $P_{\text{orb}}^{1/3}$. Note that the orbital period, P_{orb} , is very accurately measured by *Kepler*, as is the ratio of the planet's radius, R_p , to that of the star, R_{\star} , provided dilution by nearby stars is small.

Planetary transits with an impact parameter smaller than half the star's radius have a duration that exceeds $3^{1/2}/2 \approx 86.67\%$ that of a central transit. Such transits account for almost half of all transiting planets, and over half of the transits observed to a specified SNR threshold. The fraction of transits with durations greater than half that of a central transit is $3^{1/2}/2$; again specifying a SNR threshold increases the observed fraction. Orbital eccentricities also influence the durations of transits and FPs; in most cases, durations are reduced because speeds are

highest near periastron (Kepler 1609), where geometric considerations imply that transit probabilities are larger.

4. VALIDATION OF THE 5-PLANET SYSTEM KEPLER-33

There are two primary purposes of this work: demonstrating the very high credibility of the ensemble of *Kepler* multi-planet candidates and providing a framework to validate particular systems of candidates as planets. We now turn to a specific system that is both intrinsically interesting because it is the closest analog to Kepler-11 observed to date (Lissauer et al. 2011a) and has characteristics very favorable for validation by multiplicity.

KOI-707 (KIC 9458613) is a $Kp = 14$ star for which four planet candidates, ranging in period from 13 to 41 days, were announced by Borucki et al. (2011); a fifth candidate planet, with shorter orbital period and smaller size, has subsequently been identified. The lightcurve of this target is shown in Figure 2.

We performed an analysis of pixel-level *Kepler* spacecraft data that shows that the transit signals come from a location on the sky that is coincident with that of the target star within small uncertainty, and we obtained high-resolution images of the target that did not show any nearby stars capable of producing the transit signals; these studies are presented in Section 4.1. Our analyses of the transit lightcurves and spectra taken of the target star are presented in Section 4.2. In Section 4.3, we review the characteristics of this system that allow for its validation by multiplicity. We discuss the properties of the Kepler-33 planetary system in Section 4.4.

4.1. Location of Transit Signature on the Plane of the Sky

A seeing-limited image taken at Lick shows a star $7''$ to the NW that is 4.5 magnitudes fainter than KOI-707, but no stars closer to the target. On 12 June 2011, KOI-707 was imaged in the 880 nm filter ($\Delta\lambda = 50$ nm) of our speckle camera at the WIYN 3.5-m telescope located on Kitt Peak. This star showed no companions within a 2.8×2.8 arcsec region down to 3.1 magnitudes fainter than the target star; stars within $0.05''$ of the target star would not have been detected. Details of this speckle imaging data collection and reduction processes are fully described in Howell et al. (2011).

We check to see whether the transit signal is due to a source other than KOI-707 using the difference image technique described in Torres et al. (2011). This method fits the measured *Kepler* pixel response function (PRF) to a difference image formed from the average in-transit and average out-of-transit pixel images in order to calculate the position of the difference image centroid. This difference image centroid position is compared with the position of the PRF-fit centroid of the average out-of-transit image, as well as to the predicted deviations in centroid locations due to scene crowding. The results for all 5 planet candidates are presented in Table 1 and shown in Figure 3.

The uncertainty in the quarterly centroid locations displayed in Figure 3 is based upon propagating pixel-level uncertainty and does not include possible PRF fit bias. Sources of PRF fit bias include scene crowding, because the fit is of a single PRF that assumes a single star, and PRF error. The centroid offset is the difference between the positions of the centroids of the difference image and

out-of-transit images, so common biases such as PRF error should approximately cancel. There is, however, a quarter-dependent residual bias. Statistical analysis across many uncrowded *Kepler* targets indicates that the residual bias due to PRF error is zero-mean, so we average the quarterly centroid positions. Specifically, we compute a robust χ^2 minimizing best-fit position to the quarterly position data. The uncertainties of the average are estimated by taking the uncertainties of the fit and performing a bootstrap analysis. This average for each planet candidate is shown on Figure 3.

Bias due to crowding (stars close enough to the target that they contribute light observed in the aperture), however, does not cancel because, to the extent that variations in other field stars are not correlated with transits, field stars do not contribute to the difference image. This introduces a systematic bias component that remains in the average over quarters. To investigate the possibility that the observed offsets are due to crowding bias, we model the local scene using stars from the KIC and the measured PRF, induced the transit on KOI-707 with the ephemeris of each planet candidate, and performed the same PRF fit analysis on the model difference and out-of-transit images as that performed on the pixel data. If the resulting modeled average offset matches the observed average offset, then the observed offset can be explained by crowding bias.

The locations of the transit signatures (difference image centroids) of each of KOI-707's five planet candidates lie within $1''$ of the predicted position, and given the uncertainties listed in Table 1, none of the signatures are significantly offset and all are fully consistent with transits on the target star. Furthermore, the lack of near neighbor stars seen in the speckle image rules out some of the possible false positive scenarios that could produce a centroid shift of the magnitude suggested by the marginally significant offset observed.

4.2. Lightcurves, Spectra, Derived Properties

We obtained a spectrum of the target star KOI-707/Kepler-33 using the HiRES spectrometer at Keck I 10-m telescope. Classification of this spectrum using SME (Spectroscopy Made Easy, (Valenti & Piskunov 1996; Valenti & Fischer 2005)) yields the stellar parameter values shown in Table 2 (the final two columns in this table show results from constrained fits described at the end of this subsection). The mean stellar density based on spectroscopic information was estimated by matching the determined distributions of T_{eff} , $\log g$ and $[\text{Fe}/\text{H}]$ to the Yonsei-Yale evolution tracks. This allowed the determination of stellar mass and radius and mean stellar density posterior distribution based on spectroscopy. The spectrum of KOI-707 is consistent with two sets of stellar evolution tracks (Figure 4), leading to double-peaked probability distributions and asymmetric uncertainties in several stellar parameters. We plot the probability distributions of the fundamental parameters of stellar mass and age in Figure 5 and those of the stellar density, which is a key input to transit fitting, in Figure 6, and we include in Table 2 various measures of uncertainty beyond the simple standard deviation for the values of various derived stellar parameters that are either critical to the validation and properties of KOI-707 and/or distributed highly asymmetrically. Note that both solu-

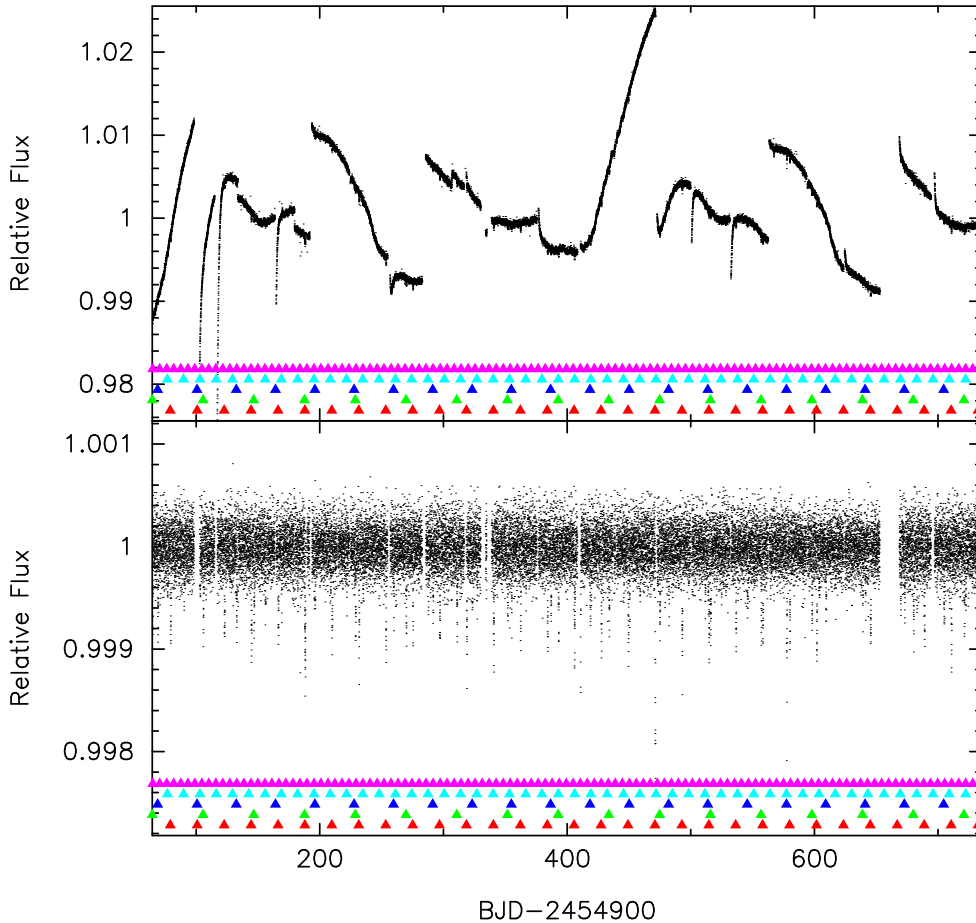


FIG. 2.— *Kepler* photometric time series data for KOI-707 (KIC 9458613; Kepler-33) in 29.426 minute intervals (standard *Kepler* long cadence observations). Calibrated data from the spacecraft with each quarter normalized to its median are shown in the top panel. The bottom panel displays the lightcurve after detrending with a polynomial filter (Rowe et al. 2010). The entire 8 Quarters of *Kepler* data analyzed herein are displayed. Note the difference in vertical scales between the two panels. The midpoint times of the five sets of periodic transits (including those that were not observed because they occurred during data gaps) are indicated by triangles of differing colors. Close-ups of folded lightcurves near transit times of each of the planets are shown in Figures 7 and 8.

tions are somewhat above the main sequence, implying an evolved star.

As an independent check of the values of the SME parameters, we also derived values by matching the spectrum to synthetic spectra (Torres et al. 2002; Buchhave et al. 2010), and in addition we employ a new fitting scheme (Stellar Parameter Classification, SPC) that is currently under development and being readied for publication, allowing us to extract precise stellar parameters from the spectra. The SPC analysis yielded the following parameters: $T_{\text{eff}} = 5849 \pm 50$ K, $\log g = 4.07 \pm 0.10$, $[\text{m}/\text{H}] = 0.12 \pm 0.08$, $v \sin i = 3.4 \pm 0.5$ km/s, $RV = 13.779 \pm 0.020$ km/s. The SME and SPC parameters are fully consistent, and the nominal value of the key parameter $\log g$ from SPC is slightly ($< 1\sigma$) larger than the SME value. In contrast, the derived stellar radius from SME is $1.82 \pm 0.16 R_{\odot}$, substantially larger (more than 3σ formal error, see Table 2) than the radius estimate of $1.29 R_{\odot}$ based upon the KIC that was used by Borucki et al. (2011).

We measured the radial velocity of KOI-707 relative to the barycenter of our Solar System. The method involves

measuring the Doppler shift of the stellar spectrum obtained with the Keck I telescope and HiRES spectrometer on BJD = 2455782.9441 relative to the solar spectrum by a χ^2 fit of the two spectra. To set the zero point of the wavelength scale accurately, we measure the displacement of telluric lines from the Earth’s atmosphere, serving as the “iodine cell”. The resulting radial velocities are accurate to 0.1 km/s, based on measurements of 2000 stars (Chubak & Marcy 2012) and comparison with IAU standard stars. For KOI-707, the radial velocity is $v_{\star} = 14.09$ km/s, indicating motion of the star away from the Solar System at a speed typical of the velocity dispersion of stars in the Galactic disk. Orbital periods of the planets quoted in Table 3 are as perceived from the barycenter of our Solar System. As the Kepler-33 system is receding from us at $4.7 \times 10^{-5}c$, where c represents the speed of light, the actual orbital periods in the rest frame of the Kepler-33 system are 0.999953 times as large as the tabulated values.

We used Q1-Q8 long-cadence *Kepler* aperture photometry (i.e., only pixel-level corrections such as bias and dark smear are applied to the data and there is no co-

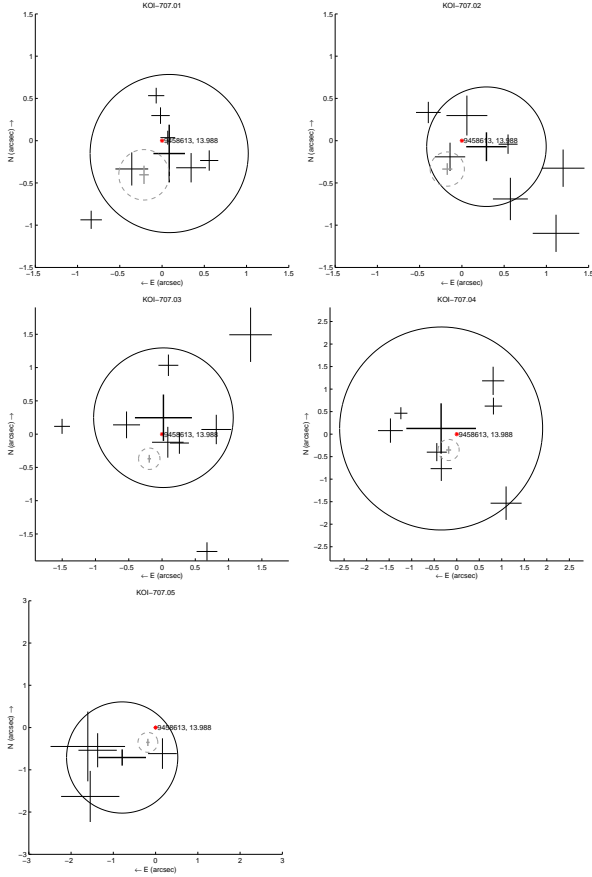


FIG. 3.— Centroid fitting results are shown for all 5 planet candidates of KOI-707. The origin is the center of light received outside of transit times. The red asterisk is the expected centroid of light during transit assuming the transit is on the target star; it is displaced from the origin because some of the light entering the aperture comes from known background stars whose brightness would not be affected by transits of the target star. (The numbers following the red asterisk are the KIC number and *Kepler* magnitude of KOI-707.) The fitted centroids of the transit signatures observed in Quarters 1 through 8 are shown as the thin black crosses, where the arms of these crosses show the uncertainty in RA and Dec. Some quarters as missing for some candidates due to failure of the PRF fit. The robust average centroid across quarters is shown by the thick black cross, with the black solid circle giving the 3σ uncertainty in the offset distance. The robust average of each modeled quarterly offsets is shown as a thick gray cross, with the gray dashed circle showing the average model 3σ offset distance uncertainty. When the circle showing the observed 3σ uncertainty in the difference image has significant intersection with the dashed circle showing the modeled 3σ uncertainty in the position of the target star, the data are consistent with the observed transit signal being on KOI-707.

detrending). At this level of data reduction, there are still instrumental artifacts on timescales similar to the planetary orbits. To detrend the data (remove long-period variations), a second-order polynomial was fitted to segments of sequential *Kepler* photometry data outside of transits (i.e., in-transit observations were given zero weight), and then this polynomial was subtracted from the data. A segment is defined as a length of data that is uninterrupted for 5 or more consecutive long cadences (~ 2.5 hours). Each segment is then combined to produce a final time series that is then normalized by the

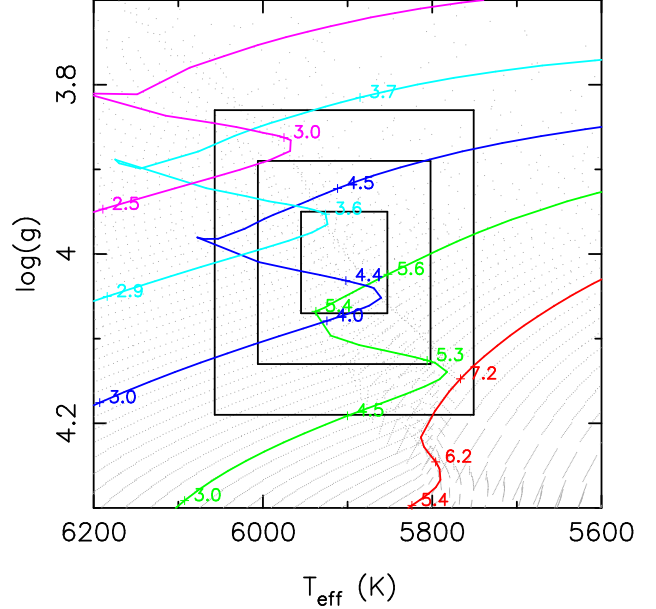


FIG. 4.— Plotted are the Yonsei-Yale evolutionary tracks for 1.1 M_{\odot} (red), 1.2 M_{\odot} (green), 1.3 M_{\odot} (blue), 1.4 M_{\odot} (cyan) and 1.5 M_{\odot} (magenta) stars with $[\text{Fe}/\text{H}] = 0.15$. Ages, in Gyr, are marked along the tracks. Note the uneven rates of evolution along these tracks. The gray dotted tracks are spaced by 0.01 M_{\odot} in stellar mass and 0.02 Gyr in time to illustrate the distribution of field stars on the $\log g - T_{\text{eff}}$ plane; the apparent gaps/discontinuities in these tracks are caused by rapid changes at various stages of stellar evolution. The three boxes mark the 1, 2 and 3 σ confidence regions of the spectroscopic SME analysis of the spectrum of KOI-707 taken at Keck. There are degeneracies in determining a unique stellar mass and radius for specified values of T_{eff} and $\log g$. For example, a 4.4 Gyr, 1.3 M_{\odot} model and a 5.5 Gyr, 1.2 M_{\odot} model have nearly identical T_{eff} and $\log g$. The low-mass/old peaks in the probability distribution functions shown in Figure 5 result from the pile-up of stellar evolution tracks as core H is exhausted in the transition regime from radiative cores of 1.1 M_{\odot} and smaller stars to convective cores in 1.2 M_{\odot} and larger stars. The high-mass/young peaks result from the overlap between tracks for the early shell H burning phase of stars with convective cores with tracks for the late core H burning phase of stars that are $\sim 0.12 M_{\odot}$ more massive.

median.

We adopt a simple model to fit the data. We fit for the mean stellar density (ρ_{\star}), and each planet's orbital period (P_{orb}), transit epoch (T_0), scaled planetary radius (R_p/R_{\star}) and impact parameter (b). The planets are assumed to be on circular orbits; planet-planet interactions are implicitly accounted for by allowing the center of transit time to vary in order to best-fit transit shape (minimization of scatter on residuals). The transit was described with the analytic formulae of Mandel & Agol (2002), and we adopted a non-linear limb darkening law with coefficients fixed based on the Claret & Bloemen (2011) tabulation for the *Kepler* band with stellar parameters from SME analysis. A best fit model was computed using a Levenberg-Marquardt algorithm to minimize the χ^2 statistic and initial uncertainties were estimated via the construction of a co-variance matrix.

The best fit model and co-variances were used to seed a hybrid-MCMC (Markov Chain Monte-Carlo) algorithm to determine posterior distributions of our model parameters. The model is considered hybrid, as we randomly

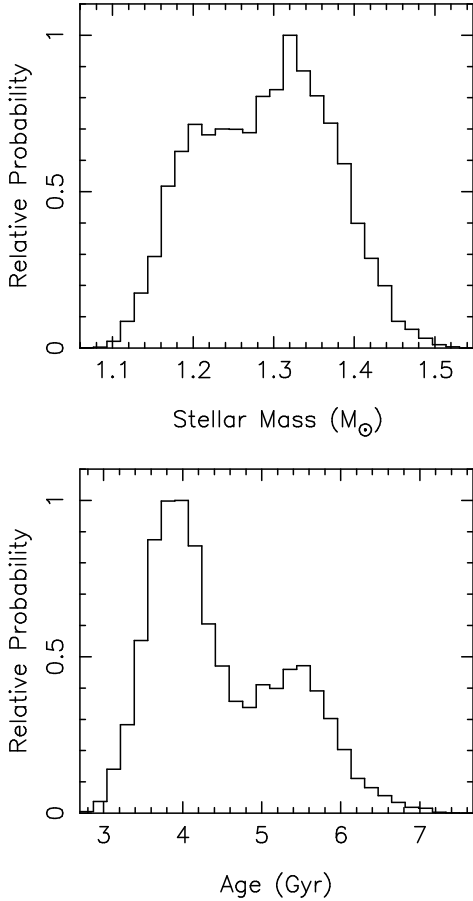


FIG. 5.— The relative probability distribution of estimates for the mass and age of the star Kepler-33 (KOI-707), computed using the SME analysis of the star's spectrum and a prior based on the frequency distribution of stars, as described in the text. Both curves are double-peaked because two solutions, both recently evolved off the main sequence, are consistent with the data. Integration under the curves implies that the younger, more massive, solution is a bit more probable than a somewhat older and fainter star.

use a Gibbs-sampler and a buffer of previous chain parameters to produce proposals to jump to a new location in the parameter space. The addition of the buffer allows for a calculation of vectorized jumps that allow for efficient sampling of highly correlated parameter space.

A direct comparison of the mean stellar density determined by the circular transit-model (0.236 ± 0.080) and the mean stellar density determined from spectroscopy (0.301 ± 0.067) differ by less than 1σ . This shows that we can produce a self-consistent circular model in which all five planets orbit the same star and produce stellar parameters that agree with spectroscopy.

Close-ups of the lightcurves of each of the planets near planetary transit are shown in Figure 7. Transit durations of all five KOIs vary in proportion to the $P_{\text{orb}}^{1/3}$ to within 5%, and to within 3% when planet sizes are factored in as specified in Expression (10). The remarkable similarity of these transit durations when appropriately scaled to orbital periods is apparent in Figure 8, which shows the same data as Figure 7 but with the time coordinate

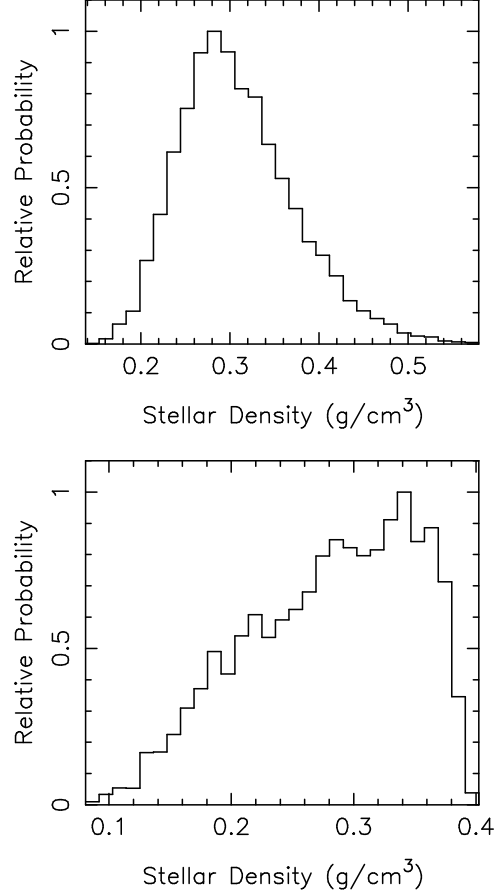


FIG. 6.— The relative probability distribution of estimates for the density of the star Kepler-33 (KOI-707). The top curve was computed using an MCMC analysis of the transit photometry data, whereas the results shown in the bottom panel incorporated the SME analysis of the star's spectrum and a prior based on the frequency distribution of stars. The spectral solution is highly asymmetric because two groups of stars are consistent with the data (see Figure 4). Note the difference in horizontal scales between the two panels.

coordinate scaled by $P_{\text{orb}}^{1/3}$. Such similarity would be the consequence of an ensemble of planets transiting the same star on low eccentricity orbits with similar impact parameters. The impact parameters given in Table 3 are indeed quite similar for all of the planets. But the inclinations implied to produce these parameters require a very fortuitous arrangement in which tilt to the line of sight is just enough larger in the inner planets than the outer ones. In contrast, if the system is viewed nearly edge on, i.e., $i \approx 90^\circ$, then both a wider range of impact parameters would be allowed (because transit durations are less sensitive to the precise value of b when $b \ll 1$) and similar values of b imply a very flat system rather than a fortuitous ensemble of tilts.

We are thus motivated to perform a second set of fits constrained by the assumptions of circular orbits for all planets and $b = 0$ for the planet with the longest normalized (according to Expression 10) transit duration, KOI-707.01. Two such fits were performed, one for the low mass stellar solution (where we imposed the constraint $M_\star < 1.21 M_\odot$) and the other for the high mass

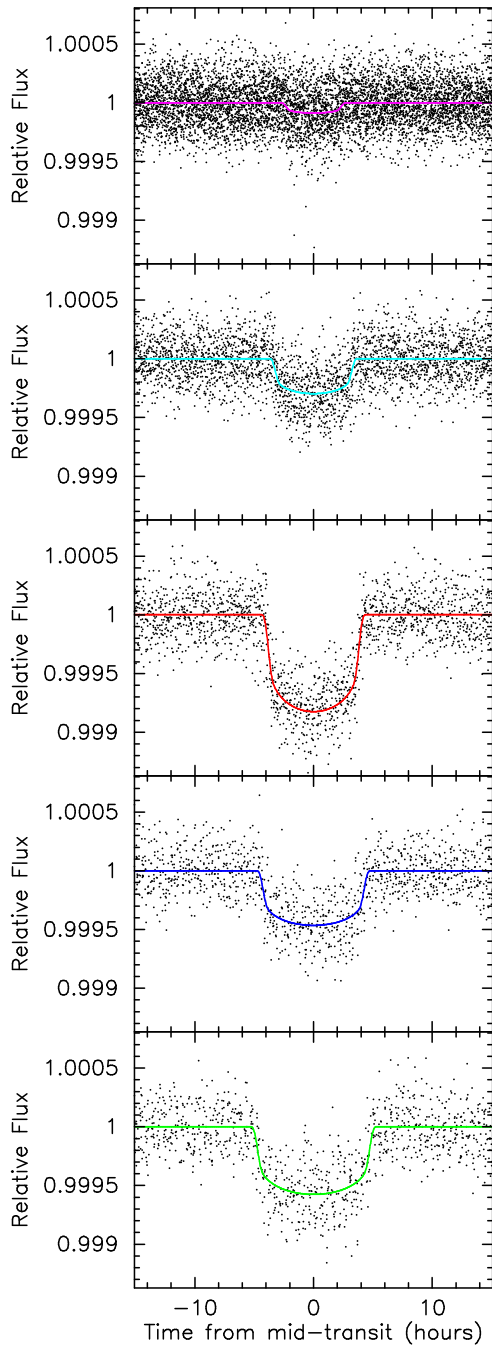


FIG. 7.— Detrended *Kepler* flux from Kepler-33 shown phased at the period of each transit signal and zoomed to a 30-hour region around mid-transit. Black dots represent individual *Kepler* long cadence observations. The folded light curves corresponding to the model fits are shown in colors that correspond to these used in Figure 2. In each panel, the best-fit model for the other 4 planets was removed before plotting. Each panel has an identical vertical scale, to show the relative depths, and identical horizontal scale, to show the relative durations.

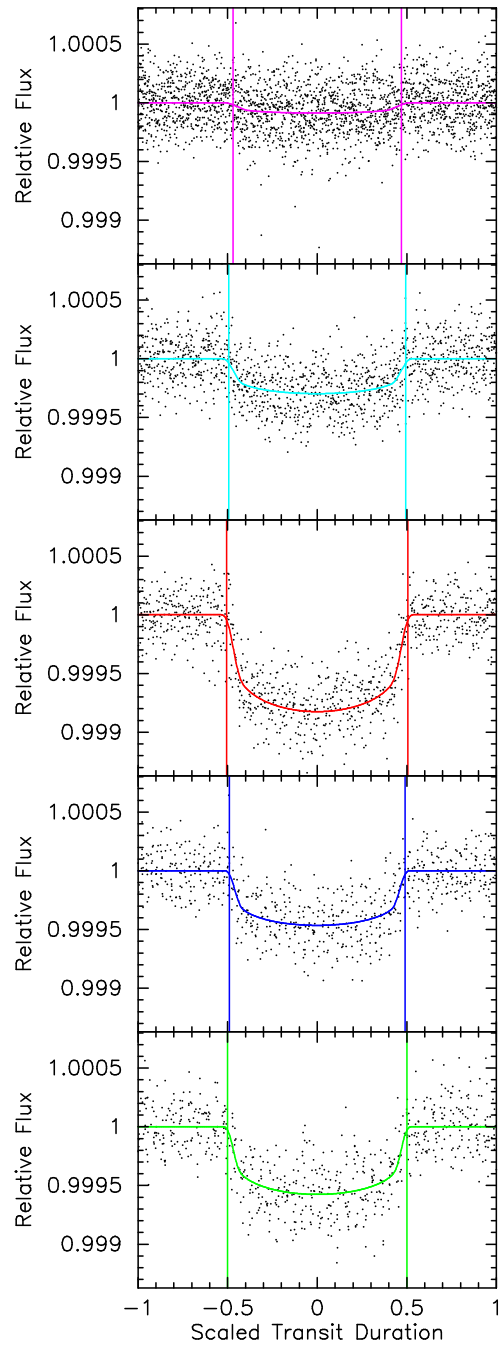


FIG. 8.— The folded lightcurves near the transit of each planet in the Kepler-33 system, as shown in Figure 7, but in this case the time coordinate in each panel has been scaled to $P_{\text{orb}}^{1/3}$ of the planet in question. Vertical lines mark the beginning and end times for each transit. For planets on circular orbits with the same impact parameter, durations normalized in this manner should be the same for all planets. The remarkable similarity in normalized durations of these planets is very strong evidence that they all orbit the same star.

($M_\star > 1.21 M_\odot$) solution. We show in the far right columns of Tables 2 and 3 both the high and low stellar mass “Flat” fits; no uncertainties are quoted for these fits because the $b = 0$ assumption constrains results so tightly that computed uncertainties are unrealistically low.

The fitting procedure that we used to compute the planetary parameters listed in Table 3 did not account for the small (1 – 2%) contribution of the second star in the aperture to the flux measured by *Kepler*. This dilution implies that the planet radii quoted are overestimated by 0.5 – 1%, a difference far smaller than the uncertainties in their actual values.

4.3. Validation of the *Kepler-33* Planetary System

The five planetary candidates of KOI-707 are extremely likely to represent a true 5 planet system orbiting the target star. There are several lines of evidence that support this conclusion. First, the analysis presented in Section 2 implies that the overwhelming majority of *Kepler* multiple-planet candidates are true planets and bound within the same physical system.

Second, the planetary system is already closely-packed dynamically for the sizes of planets around an undiluted target star (see Section 4.4). Were the planetary system to orbit another star that is not seen because it is significantly fainter than the target, the larger planets required to match the observations would necessitate implausibly low densities for the planetary system to be stable.

Third, the spatial location analysis presented in Section 4.1, combined with the galactic latitude distribution of targets and planet candidates shown in Figure 1 and the relatively high galactic latitude of KOI-707 (15°), together imply that it is unlikely that the signals are due to a source not physically associated with the target star.

Fourth, the long durations of the transits relative to the planets’ orbital periods imply that they are produced by light being blocked from a star whose density is significantly less than those of cool dwarfs, and/or they are produced by apocentric transits of objects with substantial orbital eccentricity. Substantial orbital eccentricities would make the system unstable if the planets orbited the same star. It is highly implausible that two stars in an unresolved stellar binary would be so similarly coeval to have nearly equal densities characteristic of a somewhat evolved star.

Fifth, the remarkable similarity of the transit durations when appropriately scaled to orbital periods (Expression (10) and Figure 8) can be understood as the consequence of an ensemble of planets transiting the same star with similar impact parameters, but would otherwise be an unlikely coincidence.

The above characteristics of KOI-707.01–05, combined with the overall high validity of *Kepler* multis, imply that these candidates have a well above 99% probability of composing a true multi-planet system, hence we consider these candidates to be validated planets and name the system *Kepler-33*.

4.4. Characteristics of the *Kepler-33* Planetary System

Numerical integrations to test stability of the system were performed using masses of the planets from the nominal mass-radius relationship based upon plan-

ets within our Solar System presented in Lissauer et al. (2011a). This relationship is given by:

$$M_p = \left(\frac{R_p}{R_\oplus}\right)^{2.06} M_\oplus, \quad (11)$$

where R_\oplus and M_\oplus are the radius and mass of the Earth, respectively. In previous work, Lissauer et al. (2011a) integrated the KOI-707 system using parameters based on the data presented by Borucki et al. (2011) and assuming planar initially circular orbits; the model system survived intact for the entire 3×10^8 years simulated. All of our integrations also assume that the system is planar. For all planets having zero initial eccentricity, all three models of the system listed in Tables 2 and 3 survived intact for the entire 10^7 years simulated.

Of the three *Kepler-33* planetary system models that we integrated, the one based directly on the spectroscopic stellar parameters had the largest planetary sizes and thus largest estimated planetary masses, with the fractional differences in estimated planetary masses from one model to another being larger than those for stellar mass. Thus, the spectroscopic parameters yielded the largest interplanetary perturbations, and presumably the largest TTV signatures. We examined distributions of TTV signals over 2 year periods during the first 2 Myr of this simulation. These theoretical TTVs for the inner planet were smaller than 30 seconds, and those for *Kepler-33c* less than 90 seconds, both values below current measurement capabilities. The outer three planets exhibited far larger TTVs, 9 – 18 minutes for *Kepler-33d*, 23 – 38 minutes for *Kepler-33e* and 23 – 35 minutes for *Kepler-33f*, roughly consistent with variations detected. While this model used relatively high mass estimates, the integration began with circular orbits, which produce smaller TTVs, so the results do not yield a preference between the three models of planetary sizes listed in Table 3. A detailed analysis of planetary TTVs is beyond the scope of this paper, but we note that it may well soon be possible to derive estimates of the masses of some or all of the outer three planets using observed TTVs.

The properties of the 5 planet *Kepler-33* system are analogous to those of the 6 planet *Kepler-11* system (Lissauer et al. 2011b). Both systems include 4 planets with orbital periods between 13 and 47 days that are comparable in radius to, or somewhat smaller in size than, Neptune, as well as a smaller planet closer to the star. Both systems are thus very closely-packed in a dynamical sense. The *Kepler-11* system is slightly more dynamically close-packed than is the *Kepler-33* system, both in the sense that the ratios of the orbital periods of neighboring planets are a bit larger for *Kepler-33*'s planets (Lissauer et al. 2011a) and as evidenced from smaller TTVs detected in the *Kepler-33* system.

In some aspects, the *Kepler-33* system can be viewed as a less extreme cousin of *Kepler-11*, with 5 known transiting planets rather than 6 and spacing that not quite as close, yet dynamically much tighter than most systems (Lissauer et al. 2011a). However, the new system's inner planet, *Kepler-33b*, is smaller and closer to its star than is its counterpart, *Kepler-11b*. The high density of *Kepler-11b* relative to its brethren, coupled with its smaller size, indicates a composition richer in heavy elements (Lissauer et al. 2011b). While the mass and thus

the density of Kepler-33b is not known, it is unlikely that a planet this small ($1.5 - 1.8 R_{\oplus}$) and close (0.07 AU) to its bright star ($3 L_{\odot}$) could have retained a substantial H/He atmosphere. This lends support to the suggestion by Lissauer et al. (2011b) that planets such as Kepler-11b may have once had atmospheres of light gases that subsequently escaped as a result of stellar irradiation. The slightly shorter normalized duration of the small inner planet Kepler-33b suggests that this planet has somewhat larger inclination and/or eccentricity than do the outer four planets. We note that Mercury, the innermost and smallest planet in our Solar System, also has the largest eccentricity and inclination of the 8 planets known to orbit our Sun.

Stability of the Kepler-33 planetary system excludes large eccentricities of the four outer planets, although interplanetary perturbations must cause eccentricities to be non-zero. The remarkable similarity in the normalized transit durations of the five planets orbiting Kepler-33 would be very unlikely if the eccentricities and inclinations of planetary orbits are significant (Figure 9). Moreover, the consequent similarity in computed impact parameters despite the planets’ differing orbital distances requires that either the system is viewed near edge-on, with impact parameters $b \ll 1$, or a very fortuitous coincidence producing an anticorrelation between inclinations and orbital periods. We view such a coincidence as unlikely, and therefore prefer the planetary parameters closer to those listed in final two columns of Tables 2 and 3 (the “Flat” fits) than to those listed in the second column of Tables 2 and 3.

5. CONCLUSIONS

The calculations presented in Section 2 show that the vast majority of *Kepler*’s multi-planet candidates are indeed planets. The essence of our argument is that fewer than 10^{-2} of *Kepler* targets have a planet candidate listed in Borucki et al. (2011). If 10% or fewer of these candidates are FPs, then fewer than 10^{-3} of *Kepler* targets have a false positive, and if FPs are not correlated with other planet candidates, then fewer than 10^{-5} of *Kepler*’s $\sim 160,000$ targets, i.e., a total of at most 2 targets, are expected to have a false positive as well as another transit-like signature that makes them a candidate multi-planet system. This number can be compared to 170 candidate multi-planet systems with a total of 408 planet candidates announced by Borucki et al. (2011). Accurate estimates of the false positive rate in this population require detailed analysis of both *Kepler* and ground-based data to account for the caveats expressed in Section 2.2. Nonetheless, we expect that $\gtrsim 400$ of the 408 planet candidates in multis that were announced by Borucki et al. (2011) are indeed exoplanets, although a small fraction of these planets orbit stars other than their nominal *Kepler* target star. Note that the smallest planet candidates are most prone to false positives, because low SNR limits the restrictiveness in parameter space of tests of lightcurve shape and location of the centroid of the transit signal on the sky plane, and the abundance of astrophysical signals that are capable of producing lower amplitude events is greater. Also note that stellar parameters, and thus planetary sizes, are

prone to large uncertainties for candidates that have no high-SNR spectroscopic observations from the ground.

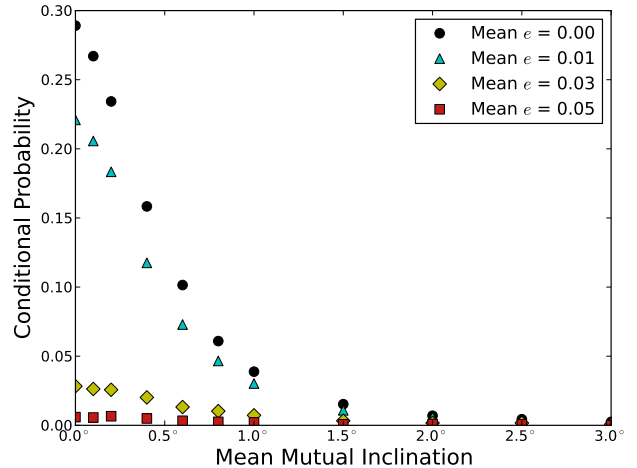


FIG. 9.— The probability of observing all five planets in the Kepler-33 system to have period-normalized transit durations within 3.0% of one another given that all five planets are seen to transit the host star is shown as a function of mean mutual inclination. Points were derived using Monte Carlo simulations that assumed parameters from the spectroscopic fit given in the second column of Tables 2 and 3. Results with the flat fit parameters (not shown) are nearly identical. Mutual inclinations for each realization are drawn from a Rayleigh distribution with respect to random reference plane (i.e., random observer). The black dots are for the $e = 0$ case. The blue triangles, yellow diamonds and red squares show results from simulations in which the eccentricity assigned to each planet was drawn from a Rayleigh distribution with mean value $\langle e \rangle = 0.01$, $\langle e \rangle = 0.03$ and $\langle e \rangle = 0.05$, respectively. The addition of even a small range of eccentricities greatly reduces probability of highly correlated transit durations.

From a Bayesian statistical perspective, multiplicity effectively allows us to increase the planet prior, and thus enables the validation of candidates as being true planets at a specified high probability level without going to the extreme lengths often required to provide a very small upper bound on the FP prior. We use these arguments along with a detailed analysis of *Kepler* data to validate the Kepler-11 analog KOI-707 system, which we name Kepler-33.

Kepler was competitively selected as the tenth Discovery mission. Funding for this mission is provided by NASA’s Science Mission Directorate. The authors thank the many people who gave so generously of their time to make the *Kepler* mission a success, chief among them Bill Borucki, who has devoted decades to developing and implementing *Kepler*. Useful comments were provided by Natalie Batalha, Ruth Murray-Clay, Dimitar Sasselov, Jason Steffen, and especially by Tim Brown. Kevin Zahnle and Mark Marley provided constructive comments on the manuscript. D. C. F. acknowledges NASA support through Hubble Fellowship grant #HF-51272.01-A, awarded by STScI, operated by AURA under contract NAS 5-26555.

TABLE 1
CENTROID OFFSETS FOR KOI-707 BASED ON PRF FITS.

Planet	Transit Offset from KOI-707 (arcsec)	Transit Offset from KOI-707 (Offset/ σ)	Transit Offset from Prediction (arcsec)	Transit Offset from Prediction (Offset/ σ)
.01	0.17 ± 0.29	0.59	0.39 ± 0.26	1.50
.02	0.30 ± 0.22	1.35	0.53 ± 0.22	2.38
.03	0.25 ± 0.39	0.63	0.65 ± 0.40	1.64
.04	0.37 ± 0.93	0.39	0.50 ± 0.67	0.75
.05	1.06 ± 0.42	2.53	0.71 ± 0.48	1.47

TABLE 2
CHARACTERISTICS OF THE STAR KEPLER-33

Parameter	Median	σ	+1 σ	-1 σ	+3 σ	-3 σ	Flat, $M_{\star} > 1.2 M_{\odot}$	Flat, $M_{\star} < 1.2 M_{\odot}$
Spectroscopy								
M_{\star} (M_{\odot})	1.291	0.082	0.063	-0.121	0.212	-0.200	1.271	1.164
R_{\star} (R_{\odot})	1.82	0.16	0.14	-0.18	0.49	-0.42	1.663	1.615
Z	0.0250	0.0019					0.0248	0.0241
T_{eff} (K)	5904	47					5899	5880
$\log(L_{\star}/L_{\odot})$	0.556	0.080					0.476	0.446
Age (Gyr)	4.27	0.87	0.74	-1.03	2.68	-1.65	4.31	5.92
$\log g$ (cm^2/s)	4.027	0.056					4.0994	4.087
v_{\star} (km/s)	14.09	0.1						
ρ_{\star} (g/cm^3)	0.300	0.066	0.049	-0.079	0.230	-0.147	0.3883	0.3885
Transit Model								
ρ_{\star} (g/cm^3)	0.288	0.081	0.091	-0.066	0.112	-0.215	0.03897	0.3897

REFERENCES

- Batalha, N. M., et al. 2010, *ApJ*, 713, 103
 Batalha, N. M., et al. 2011, *ApJ*, 729, 27
 Borucki, W. J., et al. 2011, *ApJ*, 736, 19
 Brown, T. M., Latham, D. W., Everett, M. R., & Esquerdo, G. A. 2011, *AJ*, 142, 112
 Bryson, S., et al. 2012, in preparation
 Buchhave, L. A., et al. 2010, *ApJ*, 720, 1118
 Chubak, C. & Marcy, G. W. 2012, in preparation
 Claret, A. & Bloemen, S. *A&A*, 529, 75
 Cochran, et al. 2011, *ApJS*, 197, 7
 Demory, B.-O., & Seager, S. 2011, *ApJS*, 197, 12
 Desert, J.-M. et al. 2012, in preparation
 Doyle, L. R., et al. 2011, *Science*, 333, 1602
 Fressen, F., et al. 2011, *ApJS*, 197, 5
 Graczyk, D., et al. 2011, arXiv, 1108.0446v1
 Haswell, C. A. 2011. *Transiting Exoplanets*. Cambridge University Press.
 Hayward, T. L., Brandl, B., Pirger, B., Blacken, C., Gull, G. E., Schoenwald, J., & Houck, J. R. 2001, *PASP*, 113, 105
 Holman, M. J., & Murray, N. W. 2005, *Science*, 307, 1288
 Holman, M. J., et al. 2010, *Science*, 330, 51
 Horch, E. P., van Altena, W. F., Howell, S. B., Sherry, W. H., & Ciardi, D. R. 2011, *AJ*, 141, 181
 Howard, A. W., et al. 2011, Submitted to *ApJ* (arXiv1103.2541)
 Howell, S. B., Everett, M. E., Sherry, W., Horch, E. & Ciardi, D. M. 2011, *AJ*, 142, 19
 Jenkins, J. M., et al. 2010, *ApJ*, 713, L87
 Kepler, J. 1609, *Astronomia Nova*, Heidelberg
 Kepler, J. 1619, *Harmony of the World*, Linz
 Latham, D. W., et al. 2011, *ApJ*, 732, 24
 Lissauer, J. J., et al. 2011a, *ApJS*, 197, 8
 Lissauer, J. J., et al. 2011b, *Nature*, 470, 53
 Mandel, K., & Agol, E. 2002 *ApJ*, 579, L171
 Morton, T. D., & Johnson, J. A. 2011, *ApJ*, 738, 170
 Ragozzine, D., & Holman, M. J. 2010, submitted to *ApJ*, arXiv:1006.3727
 Robin, A. C., Reylé, C., Derrière, S. & Picaud, S. 2003, *A&A*, 409, 523
 Robin, A. C., Reylé, C., Derrière, S. & Picaud, S. 2004, *A&A*, 416, 157
 Rowe, J. F., et al. 2010, *ApJ*, 713, 150
 Seager, S., & Mallén-Ornelas, G. 2003, *ApJ*, 585, 1038
 Torres, G., Neuhauser, R., & Guenther, E. W. 2002, *AJ*, 123, 1701
 Torres, G., et al. 2011, *ApJ*, 727, 24
 Troy, M. et al. 2000, *Proc. SPIE*, 4007, 31
 Valenti, J. A. & Piskunov, N. 1996, *A&AS*, 118, 595
 Valenti, J. A. & Fischer, D. A. 2005, *A&AS*, 159, 141
 Wright, J. T., Upadhyay, S., Marcy, G. W., Fischer, D. A., Ford, E. B., & Johnson, J. A. 2009, *ApJ*, 693, 1084
 Wright, J. T., et al. 2011, *ApJ*, 730, 93

TABLE 3
CHARACTERISTICS OF THE KEPLER-33 PLANETS

Parameter	Median	σ	+1 σ	-1 σ	+3 σ	-3 σ	Flat, $M_\star > 1.2 M_\odot$	Flat, $M_\star < 1.2 M_\odot$
Kepler-33b = KOI-707.05								
T_0 (BJD-2454900)	64.8981	0.0075					64.8973	64.8973
P_{orb} (days)	5.66793	0.00012					5.667939	5.667939
b	0.50	0.16	0.16	-0.20	0.34	-0.41	0.298	0.298
R_p/R_\star	0.00877	0.00046					0.00853	0.00853
R_p (R_\oplus)	1.74	0.18					1.549	1.504
i (degrees)	86.39	1.17	0.96	-1.62	2.90	-3.16	88.03	88.03
a/R_\star	7.87	0.87					8.714	8.714
a (AU)	0.0677	0.0014					0.06740	0.06544
Tr_{depth} (ppm)	86.8	6.8					87.7	87.7
Tr_{dur} (hr)	4.88	0.16	0.16	-0.15	0.45	-0.54	4.80	4.80
Kepler-33c = KOI-707.04								
T_0 (BJD-2454900)	76.6764	0.0042					76.6777	76.6777
P_{orb} (days)	13.17562	0.00014					13.17563	13.17563
b	0.44	0.17	0.17	-0.21	0.38	-0.38	0.144	0.144
R_p/R_\star	0.01602	0.00057					0.01560	0.01560
R_p (R_\oplus)	3.20	0.30					2.833	2.751
i (degrees)	88.19	0.72	0.58	-1.06	1.55	-1.92	89.46	89.46
a/R_\star	13.8	1.5					15.292	15.292
a (AU)	0.1189	0.0025					0.11287	0.11484
Tr_{depth} (ppm)	297.7	9.1					299.8	299.8
Tr_{dur} (hr)	6.700	0.104	0.096	-0.107	0.325	-0.295	6.616	6.616
Kepler-33d = KOI-707.01								
T_0 (BJD-2454900)	122.6342	0.0018					122.6341	122.6341
P_{orb} (days)	21.77596	0.00011					21.775984	21.7759
b	0.44	0.17	0.14	-0.23	0.38	-0.40	0 (assumed)	0 (assumed)
R_p/R_\star	0.02667	0.00087					0.02589	0.02589
R_p (R_\oplus)	5.35	0.49					4.700	4.564
i (degrees)	88.71	0.51	0.61	-0.48	1.08	-1.37	90 (assumed)	90 (assumed)
a/R_\star	19.3	2.1					21.38	21.38
a (AU)	0.1662	0.0035					0.16533	0.16053
Tr_{depth} (ppm)	831.4	10.5					831	831
Tr_{dur} (hr)	8.011	0.097	0.065	-0.103	0.345	-0.192	7.987	7.987
Kepler-33e = KOI-707.03								
T_0 (BJD-2454900)	68.8715	0.0048					68.8720	68.8720
P_{orb} (days)	31.78440	0.00039					31.78438	31.78438
b	0.47	0.16	0.14	-0.21	0.38	-0.37	0.204	0.204
R_p/R_\star	0.02011	0.00072					0.01955	0.01955
R_p (R_\oplus)	4.02	0.38					3.550	3.446
i (degrees)	88.94	0.37	0.45	-0.35	0.84	-1.07	89.576	89.576
a/R_\star	24.9	2.8					27.51	27.51
a (AU)	0.2138	0.0045					0.2127	0.20656
Tr_{depth} (ppm)	467	12					469	469
Tr_{dur} (hr)	8.90	0.13	0.12	-0.13	0.40	-0.38	8.819	8.819
Kepler-33f = KOI-707.02								
T_0 (BJD-2454900)	105.5763	0.0040					105.5757	105.5757
P_{orb} (days)	41.02902	0.00042					41.02903	41.02903
b	0.43	0.17	0.15	-0.23	0.39	-0.42	0.130	0.130
R_p/R_\star	0.02227	0.00076					0.02171	0.02171
R_p (R_\oplus)	4.46	0.41					3.941	3.827
i (degrees)	89.17	0.34	0.33	-0.42	0.68	-0.98	89.772	89.772
a/R_\star	29.5	3.3					32.61	32.61
a (AU)	0.2535	0.0054					0.2522	0.2449
Tr_{depth} (ppm)	579	12					581	581
Tr_{dur} (hr)	9.87	0.13	0.11	-0.15	0.43	-0.36	9.732	9.732